Optimized Immobilization of Biomolecules on Nonspherical Gold Nanostructures for Efficient Localized Surface Plasmon Resonance Biosensing

analytical chemistry

Article

Cite This: Anal. Chem. 2019, 91, 15090−15098

pubs.acs.org/ac

Optimized Immobilization of Biomolecules on Nonspherical Gold Nanostructures for Efficient Localized Surface Plasmon Resonance Biosensing

Ainash Garifullina and Amy Q. Shen*

Micro/Bio/Nanofluidics Unit, Okinawa Institute of Science and Technology Graduate University, 1919-1 Tancha, Onna-son, Okinawa 904-0495, Japan

Supporting Information

ABSTRACT: Plasmonic biosensing techniques employ metal nanostructures, commonly gold (Au), often with biomolecules attached to their surfaces either directly or via other linkers. Various surface chemistry methods based on dispersion and covalent interactions are used to attach biomolecules to Au. As a result, when immobilizing a molecule on a metal surface, quantitative estimates of binding efficiency and stability of these surface chemistry methods are needed. Most prior work to compare such methods deals with bulk/thin film configurations or spherical nanoparticles, and very little is known about immobilization of biomolecules on plasmonic nanostructures of different shapes. Besides, due to rapid advancement of modern nanofabrication techniques, there is a growing need to determine an efficient surface chemistry method for immobilization of biomolecules on nonspherical plasmonic nanostructures. Previous comparison of immobilization methods on spherical Au nanoparticles has shown that physical adsorption resulted in the highest concentration of immobilized antibodies. In our work, we conducted a similar study and compared four representative Au surface functionalization methods as well as estimated how efficient these methods are at attaching biomolecules to nonspherical plasmonic Au nanostructures. We estimated the concentration of immobilized antibody that is specific to human C-reactive protein (anti-hCRP) by measuring the localized surface plasmon resonance (LSPR) shifts after exposing the surface of Au nanostructures to the antibody. Our results differ from the previously reported ones since the highest concentration of anti-hCRP was immobilized using 11-mercaptoundecanoic acid (MUA) chemistry. We demonstrated that immobilized antibodies retained their stability and specificity toward hCRP throughout the immunoassay when diluted hCRP or hCRP-spiked human serum samples were used. These findings have important implications for the fields of biosensing and diagnostics that employ nonspherical plasmonic nanostructures since an overall performance of these devices depends on efficient biomolecule immobilization.

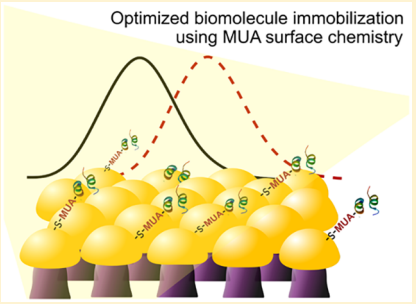

Proteins are crucial for catalysis of metabolic reactions, defense against viruses and bacteria, signal transduction within and between cells, transport of biomolecules, and cell movement, to mention just a few functions.[1−3] One strategy to investigate biomolecules and their bioactivity is to examine interactions between light (photons) and surrounding matter (i.e., biological samples). These studies offer insights about molecular function by evaluating changes in energy levels of light upon sample exposure.[4] One technique for studying light−matter interactions is localized surface plasmon resonance (LSPR) spectroscopy, which quantifies collective resonance of free electrons on metal surfaces stimulated by incident light when nanostructures are smaller in size than the wavelength of the incoming light.[5] Existing LSPR protein detection and analytical systems are influenced by employed surface chemistry method, which, in turn, is affected by the substrate surface, shape, functional groups of immobilized biomolecules, as well as by conditions of incubation steps.[6−9] Poor immobilization may lead to changes in protein conformation or structural modifications that reduce its overall bioactivity.[10,11] Therefore, optimization of surface chemistry for maximum protein immobilization and retention of its bioactive structure is critical.[12,13] While there have been comparative studies performed on individual Au nanoparticles, our work builds upon this research by comparing biomolecule immobilization methods using nonspherical plasmonic nanostructures. Ciaurriz et al. compared immobilization of biomolecules on spherical Au nanoparticles by means of physical adsorption, methyl−PEG−thiol linkers, and hydrazine dithiol linkers, and reported that simple adsorption resulted in the most efficient functionalization of spherical Au nanoparticles.[14] However, a similar study on functionalization of nonspherical nanostructures is needed since it has been shown that modifying aspect ratios and shapes of plasmonic nanostructures increases their refractive index unit sensitivity leading to improved levels of biosensing.[15] This, in turn, leads to development of both chemical and physical nanofabrication techniques to produce nanostructures with increased variety of

Received: August 18, 2019
Accepted: November 6, 2019
Published: November 6, 2019

shapes and sizes.[16] Thus, we compared performance of four representative Au functionalization methods based on results of an antibody immobilization on the surface of Au caps positioned on silicon oxide nanocones.

Gold (Au) is the most commonly used noble metal in plasmonic biosensing since it is chemically stable in air and compatible with most biomolecules.[17−19] Accordingly, we chose Au nanostructures (AuNS) as a benchmark platform for systematic studies of representative biomolecule immobilization methods. Human C-reactive protein (hCRP) and its respective antibody (anti-hCRP) were chosen as a model protein system since hCRP with its antibody are regularly used for protein binding assays.[20] To immobilize anti-hCRP on AuNS, we used four common Au functionalization techniques. In the first method, proteins are attached to AuNS by means of simple physical adsorption (referred to as the adsorption method), performed by drop-casting a diluted protein solution on the AuNS surface. Binding is based on dispersion forces between biomolecules and the sensor surface. Although this method is simple and quick, proteins are often immobilized in random orientations and tend to deattach during changing of incubation media or rinsing of the sensor surfaces.[21] In the second method, in microcontact printing (μCP method), the antibody solution is used as ink and is first uniformly spread over the poly(dimethylsiloxane) (PDMS) stamp, which is later used to transfer proteins onto the substrate. This method requires significantly less product and time and produces uniform layers of primary antibodies.[22] The third and fourth immobilization methods utilize linkers that have thiol (−SH) groups at one end and carboxyl groups (−COOH) at the other end, such as 11-mercaptoundecanoic acid (MUA method) and thiolated PEG acid linkers (HS−PEG−COOH method), respectively. These methods attach biomolecules by means of favorable interactions of Au with a sulfur atom (S) contained in the thiolated ends of these linkers. This ensures orientation-controlled immobilization of these linkers since they attach to Au via their −SH ends and with their carboxyl ends pointing away from the Au surface. Later, carboxyl groups of thiolated linkers are activated to initiate binding of the biomolecules to Au through these linkers. In our work, in addition to introducing nonspherical Au nanostructures, we incorporate an immobilization method based on self-assembly of thiolated linkers with a longer uniform molecule length (MUA) than has previously been reported by Ciaurriz et al.[14] Au and S are both large polarizable atoms that spontaneously form strong covalent bonds with each other.[23,24] For this purpose, the Au surface is commonly coated with biomolecules having both thermodynamically and sterically available thiol functional groups.[25,26] As a consequence, Au−S immobilization methods are expected to produce more strongly linked and uniformly oriented protein layers. However, a quantitative comparison of these four immobilization techniques is needed since efficient binding of molecules has a potential to improve sensitivity and to lower both limits of detection (LOD) and quantification (LOQ) of biosensing devices.

In this work, in addition to common immobilization methods based on physical adsorption or thiolated PEG acid linkers, we introduced a surface chemistry method with controlled transfer of biomolecules onto a substrate, μCP, and another immobilization method via longer thiolated linkers with uniform chain length, 11-mercaptoundecanoic acid (MUA). We used detected LSPR shifts to estimate the concentration of anti-hCRP immobilized on AuNS using listed surface chemistry methods in order to identify the most efficient one. Eventually, we verified stability and specificity of the immobilized antibody to ensure that anti-hCRP remains bioactive and retains its specificity to hCRP; we also demonstrated that antibodies immobilized via MUA method can be efficiently used for hCRP sensing in human serum samples.

EXPERIMENTAL SECTION

Materials. Silicon wafers coated with a SiO_2 layer were ordered from University Wafer (Massachusetts, U.S.A.). C-Reactive protein, human serum (≥99%, CAS no. 9007-41-4) was purchased from Merck Millipore (Tokyo, Japan). Human CRP antibody (MAB 17073), human CRP biotinylated antibody (BAM 17072), and recombinant human interleukin-6 protein (IL-6, 206-IL/CF) were purchased from R&D Systems (Minnesota, U.S.A.). Tween20 (CAS no. 9005-64-5), bovine serum albumin (BSA, ≥ 96%, CAS no. 9005-64-5), phosphate buffer saline (PBS, MFCD 00131855), ethanol (95%, CAS no. 64-17-5), 11-mercaptoundecanoic acid (MUA, 98%, CAS no. 71310-21-9), 6-mercapto-1-hexanol (MCH, 97%, CAS no. 1633-78-9), 1-ethyl-3-(3-(dimethylamino)-propyl)carbodiimide hydrochloride (EDC, CAS no. 25952-53-8), and *N*-hydroxysuccinimide (NHS, 98%, CAS no. 6066-82-6) were purchased from Sigma-Aldrich (Tokyo, Japan). The PDMS elastomer kit was purchased from Dow Sylgard 184 (Wisconsin, U.S.A.). Thiol PEG acid (HS−PEG−COOH, MW 5000, PG2-CATH-5K-2) and thiol PEG thiol (HS−PEG−SH, MW 2000, PG2-TH-2K) were ordered from e-Nacalai (Tokyo, Japan). Human CRP-spiked human serum (ST-8007X4) was provided by LSI Medience Corporation (Tokyo, Japan). Deionized (DI) water from an 18.2 MΩ·cm^{-1} Milli-Q Integral 3 water purification system (Millipore, Germany) was used as a rinsing solution.

Device Fabrication and Measurement Setup. Silicon wafers with 500 nm of thermal oxide on top were coated with 4 nm of atomic Au using an e-beam evaporator (PLASSYS Bestek, France), followed by thermal dewetting at 560 °C for 3.5 h. Next, substrates were placed into an inductively coupled plasma−chemical vapor deposition (ICP−CVD, Oxford Instruments Plasma Technology, England) system (SF_6, 45 sccm) for 5 min. The resulting nanostructures were shaped as SiO_2 nanocones coated with spherical AuNS (Figure 1).[27]

Sensor Functionalization. In all experiments, anti-hCRP was diluted to 100 ng/mL in 0.01 M PBS. Between incubation steps, the sensor surface was first rinsed with wash buffer (0.01 M PBS plus 0.05% Tween20 detergent), and then with Milli-Q water. All functionalized sensor surfaces were blow-dried with compressed N_2 gas, and UV−vis signals were detected using a UV−vis spectrophotometer (Ocean Optics, Japan).

Physical Adsorption Methods. In the simple adsorption method (adsorption), substrates were incubated in anti-hCRP solution for 2 h at 4 °C on a shaker. In the μCP method, a PDMS stamp was first inked with 20 μL of 100 ng/mL anti-hCRP antibody solution for 10 min under an O_2 plasma activated coverslip (Figure S1).[28] Next, the stamp was rinsed with 0.01 M PBS and 18.2 MΩ·cm^{-1} Milli-Q water, dried with N_2, and contacted with the surface of Au-coated silica nanocones for 2 s.

Covalent-Linking Methods. For the MUA method, the sensors were first incubated (overnight, RT) in 1 M/9 M solution of MUA/MCH, and then in 1 mM MCH (1 h, RT).[29,30] Then, the −COOH ends of MUA were activated via

DOI: 10.1021/acs.analchem.9b03780
Anal. Chem. 2019, 91, 15090−15098

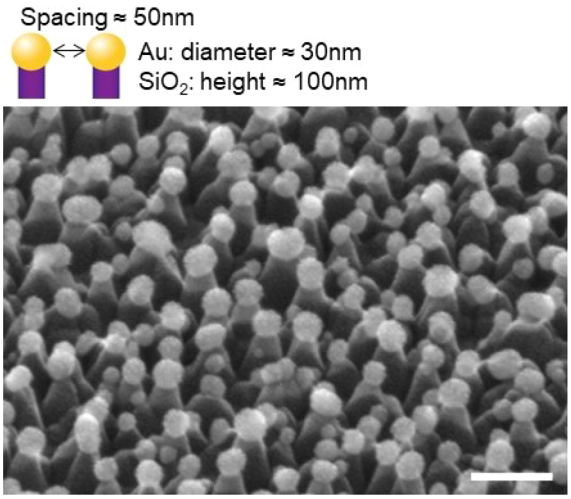

Figure 1. SEM image (1400× magnification using an FEI Quanta 250 FEG) of Au-capped SiO_2 nanocones prepared by deposition of 4 nm of Au on silicon wafers coated with 500 nm of thermal oxide, followed by 3.5 h of thermal dewetting at 560 °C and SF_6 etching (5 min). Scale bar = 100 nm.

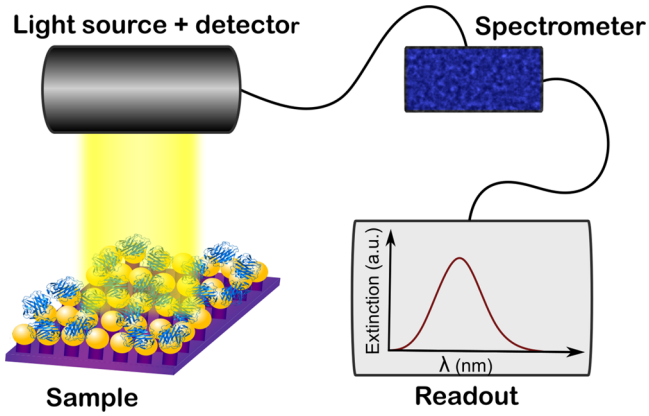

Figure 2. Measurement setup: tungsten halogen light source (HL-2000-HP-FHSA Ocean Optics, Japan) emits light on the sample surface that reflects back to the detector, and then to the spectrometer (USB4000-UV-VIS-ES Ocean Optics, Japan); recorded signal is visualized as a UV−vis spectrum from 200 to 850 nm range and is analyzed using SpectraSuite spectrometer operating software (Ocean Optics, Japan).

carboxyl-to-amine cross-linking by incubating thiolated substrates in a 4 M/1 M mixture of EDC and NHS (15 min, RT), followed by anti-hCRP for 2 h at 4 °C on a shaker.[31] In the HS−PEG−COOH immobilization technique, substrates were incubated in an 15/85 mixture of HS−PEG−COOH/HS−PEG−SH (overnight, RT), followed by backfilling with 1 μM HS−PEG solution (1 h, RT) and further activation of −COOH using EDC/NHS (4 M/1 M, 15 min, RT) chemistry and incubation in anti-hCRP solution for 2 h at 4 °C.[32]

Negative Control Systems. For the first control system, a bare Au-coated SiO_2 substrate was blocked with 0.01% BSA, followed by incubation in 100 ng/mL hCRP (1.5 h, 4 °C), and then in 100 ng/mL biotinylated anti-hCRP (1.5 h, 4 °C). For the second control, a fully BSA-coated sensor was directly incubated in 100 ng/mL solution of biotinylated anti-hCRP (2 h, 4 °C).

Stability Analysis and Sensor Specificity. To identify whether immobilized anti-hCRP was bioactive, sensor surfaces were sequentially incubated in 0.01% BSA solution (2 h, RT), 100 ng/mL hCRP solution (2 h, 4 °C), and 100 ng/mL biotinylated anti-hCRP (1.5 h, 4 °C). For devices' specificity analysis, sensors were incubated in 100 ng/mL solution of nonspecific IL-6 (2 h, 4 °C) instead of hCRP. Lastly, LOD and LOQ of the sensors were identified by incubating devices in five different concentrations of hCRP (100 pg/mL, 1 ng/mL, 10 ng/mL, 100 ng/mL, and 1 μg/mL).

RESULTS AND DISCUSSION

Immobilization Results. The UV−vis spectra of AuNS surfaces before and after anti-hCRP immobilization were acquired using the measurement setup shown in Figure 2. The maximum peak values of the recorded UV−vis spectra correspond to the maximum λ_{LSPR} that indicates the resonant wavelength at which AuNS surface electrons oscillate. The exact maximum λ_{LSPR} value varies depending on the shape, size, aspect ratio, and material composition of the nanostructures.[33−35] For instance, it has been demonstrated that increasing the size and aspect ratio of nanostructures commonly makes surface electrons resonate at a lower frequency, i.e., causes a red shift in λ_{LSPR}.[36−38] Gans' theory states the relationship between resonant wavelength λ_{LSPR} and all other important parameters, such as aspect ratio of nanostructures, dipole moments, and dielectric constants of metal and surrounding media:

$$\lambda = \frac{2\pi NV\varepsilon_m^{3/2}}{3\gamma}\sum_j \frac{(1/P_j^2)\varepsilon_2}{\left(\varepsilon_1 + \frac{1-P_j}{P_j}\varepsilon_m\right)^2 + \varepsilon_2^2} \quad (1)$$

where N is the number of particles and V is the volume of each particle, ε_m is the dielectric constant of the medium, γ is the extinction coefficient, ε_1 and ε_2 are the real and complex parts of the material's dielectric function. P_j is the depolarization constant that depends on aspect ratio of the nanostructures.[37,39] Therefore, if all parameters are kept constant except for the dielectric constant of the medium ε_m, we can calculate changes of the dielectric constant and relate that to fluctuations in the refractive index n of the medium since $\varepsilon_m = n + ik^2$, where n is the refractive index and k is the propagation wavevector.[40] Since λ_{LSPR} has a linear dependence on n, shifts in λ_{LSPR} are commonly used to detect shifts in n of a sample and, as a consequence, to estimate concentrations of various analytes.[41] Provided that the only parameter changing between the measurements is concentration of an analyte, the detected $\Delta\lambda_{LSPR}$ is related to the quantity of an analyte in the proximity of the nanostructures' surface.[36,42] That is, binding of biomolecules to a nanostructure shifts λ_{LSPR} so that the concentration of the analyte can be calculated precisely (Figure 3).[43] Therefore, in our work, $\Delta\lambda_{LSPR}$ measured after incubation of AuNS in anti-hCRP depends on the concentration of primary antibody attached to AuNS. This shift was used to estimate the primary antibody immobilization efficiency of the selected four representative Au surface chemistry methods.

In this context, immobilization efficiency is related to the number of anti-hCRP molecules that remain attached to the sensor surface after incubation of AuNS substrate in the primary antibody solution and rinsing it with PBS and Milli-Q water. Immobilization efficiency is related to the percentage of biomolecules attached to the metal surface, which can be expressed as follows:

DOI: 10.1021/acs.analchem.9b03780
Anal. Chem. 2019, 91, 15090−15098

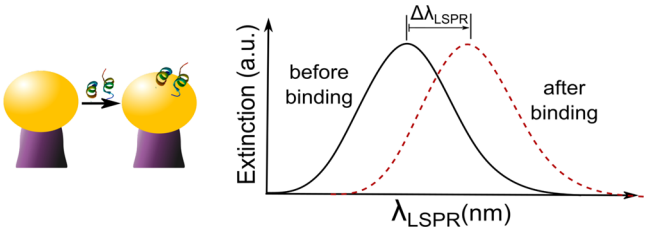

Figure 3. Electrons on the surface of a bare Au nanostructure resonate at a specific λ_{LSPR} (before binding); this λ_{LSPR} varies depending on the shape, size, and composition of the nanostructures as well as being affected by the environment surrounding these nanostructures. Binding of biomolecules changes the refractive index of the surrounding media around these nanostructure and, as a consequence, shifts λ_{LSPR} at which surface electrons resonate (after binding).

$$\text{immobilization efficiency} = \frac{C_{\text{attached}}}{C_{\text{initial}}} \times 100\% \propto \Delta\lambda_{LSPR} \quad (2)$$

A surface chemistry method that immobilizes the largest concentration of anti-hCRP was expected to display the largest $\Delta\lambda_{LSPR}$ and, as a consequence, the highest immobilization efficiency. Four immobilization methods that we analyzed resulted in different values of $\Delta\lambda_{LSPR}$ which implies that a different number of the primary antibody molecules was attached to AuNS although the same initial concentration of anti-hCRP was used in each method. Therefore, these methods are characterized by different immobilization efficiencies (eq 2) and can be compared to each other.

A wavelength shift caused by immobilization of anti-hCRP on a bare AuNS substrate is demonstrated in Figure 4a as a difference between two UV−vis spectra measured before and after incubation of AuNS in anti-hCRP solution. These differences in the λ_{LSPR} values from before and after antibody immobilization are then collected from repetitive measurements and plotted in Figure 4b with their standard deviations (see Table 1). To find if these methods were significantly different from each other, we compared their mean values by applying the analysis of variance (ANOVA) statistical test. According to ANOVA results, p- and F-values were equal to 0.001 and 10.2 for selected value of $\alpha = 0.05$, respectively. On the basis of the p-value being smaller than 0.05 and the F-value being greater than F-critical (F-critical = 3.24), the Null hypothesis can be rejected since at least two immobilization methods have significantly different mean values. Two-sample t tests and p-value comparisons can be found in Table S1.

Immobilization of anti-hCRP using MUA linkers led to the largest $\Delta\lambda_{LSPR}$ with the smallest standard deviation (13.60 ± 1.02 nm), implying that this Au functionalization method resulted in the highest concentration of immobilized anti-hCRP and therefore had the highest immobilization efficiency (eq 2). Thiol, −SH, functional groups present on MUA molecules spontaneously form covalent bonds with AuNS due to high affinity between Au and S atoms.[44,45] Moreover, proteins immobilized using covalent interactions are expected to stay attached longer due to higher resistance to washing and blow-drying of the sensor surface. Adsorption and μCP, on the other hand, are based on weak dispersion interactions between AuNS and the primary antibody, which is why they were found to have lower immobilization efficiency (see Figure 4b and Table 1). In addition, since formation of dispersion forces is highly dependent on the substrate property, the nonspherical shape of AuNS is directly related to nonuniformity of the sensor surface. Highly variable μCP results are explained by the fact that transfer of anti-hCRP from the PDMS stamp to AuNS caused damage to the sensor surfaces. Fragility of fabricated nanostructures was problematic since direct contact between the PDMS stamp and the sensor surface removed some of the nanostructures. Removed nanostructures could be later observed on the surface of the PDMS stamp (Figure S2). Since the sensor surface is composed of an array of closely located LSPR nanostructures, the final LSPR signal detected from the sensor surface is affected by plasmonic coupling between nanostructures in close proximity to each other. Consequently, removal of a small patch of AuNS due to a direct contact with the PDMS stamp caused a unique modification of the entire sensor surface in each case. This, as a result, leads to poorly reproducible immobilization results by using the μCP method since sensor surfaces were different after stamping the AuNS in every replication of $\Delta\lambda_{LSPR}$ measurements. On the basis of these results, the MUA method

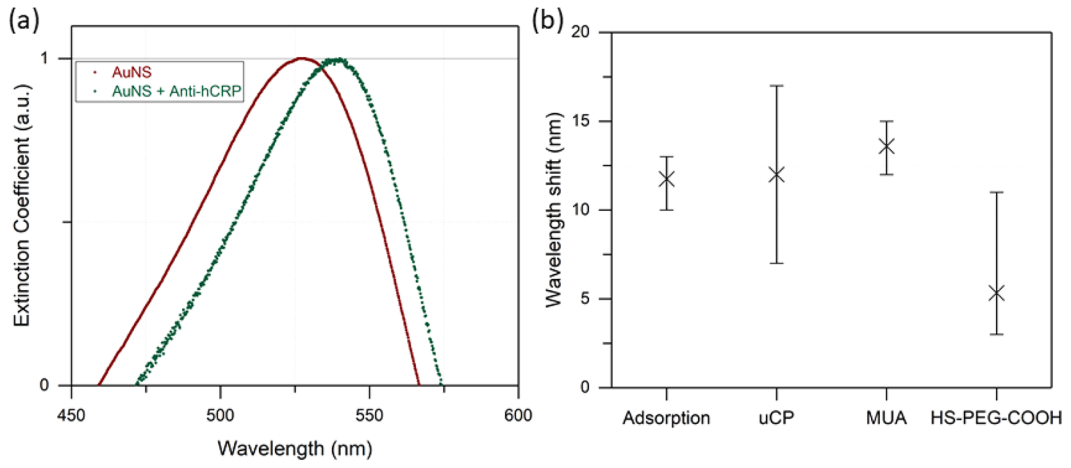

Figure 4. (a) UV−vis spectra recorded from bare Au nanostructures (red) and after immobilization of 100 ng/mL anti-hCRP on AuNS (green): functionalization of AuNS with anti-hCRP made the whole spectrum shift to the right. (b) $\Delta\lambda_{LSPR}$ (nm) averaged over eight runs of immobilization of anti-hCRP using adsorption, μCP, MUA, and HS−PEG−COOH linkers. The MUA immobilization method gave the largest $\Delta\lambda_{LSPR}$ with the smallest standard deviation (13.60 ± 1.02 nm) (i.e., had the highest immobilization efficiency).

DOI: 10.1021/acs.analchem.9b03780
Anal. Chem. 2019, 91, 15090−15098

Table 1. $\Delta\lambda_{LSPR}$ Detected after Incubation in a 100 ng/mL Solution of anti-hCRP (2 h, 4 °C)

immobilization method	adsorption	μCP	MUA	HS−PEG−COOH
$\Delta\lambda_{LSPR}$ (nm)	11.8 ± 1.1	12.0 ± 3.3	13.6 ± 1.0	5.33 ± 2.9

leads to the highest concentration of immobilized anti-hCRP (i.e., the highest immobilization efficiency). Thus, the MUA immobilization method is recommended for attaching of anti-hCRP to the nonspherical AuNS surfaces.

Stability Analysis. Efficient initial immobilization of anti-hCRP on AuNS does not always prevent deattachment of molecules during washing, transferring media, and measuring UV−vis signals. Therefore, to perform a complete stability analysis, standard sandwich-type protein detection assays were performed (Figure 5).[46] In this context, stability refers to the duration of the antibody attachment onto the sensor surface when the latter is subjected to protein binding immunoassay involving repetitive changes of the incubation media, rinsing, and blow-drying of the sensor surface.

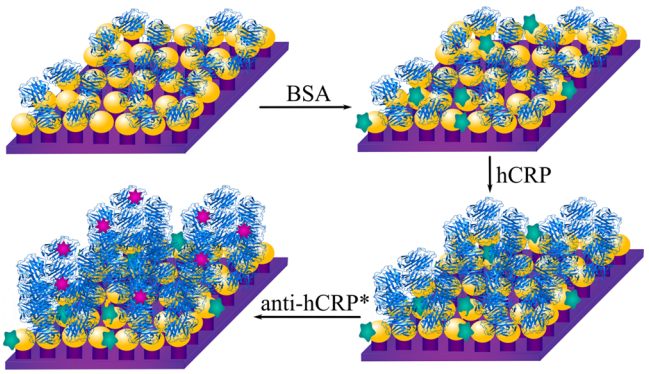

Figure 5. Functionalization of Au nanostructures with anti-hCRP was followed by incubation in 0.01% BSA (2 h, RT), 100 ng/mL hCRP (2 h, 4 °C), and biotinylated anti-hCRP (anti-hCRP*, 1.5 h, 4 °C). UV−vis spectra were recorded after each protein immobilization step.

To minimize false positive measurements as well as to prevent biofouling of molecules, we introduced two negative control systems using 0.01% BSA blocking buffer.[47] These control systems were performed by initially coating the entire sensor surface with 0.01% BSA solution. Provided that the blocking buffer is active, the sensor surface was expected to be fully coated with BSA which would prevent subsequent linking of biomolecules (i.e., hCRP and biotinylated anti-hCRP). In both cases, BSA-blocked sensors after incubation in protein solutions of hCRP and biotinylated anti-hCRP resulted in negligible $\Delta\lambda_{LSPR}$ (see Figure 6 and Table 2) suggesting that BSA successfully blocks the sensor surface and averts nonspecific binding of both antigen and biotinylated antibody to AuNS. Therefore, BSA solution was proven to be effective at preventing false positive signals and, for further stability analysis of sensors functionalized with anti-hCRP, sensors were then incubated in BSA, hCRP, and biotinylated anti-hCRP.

To test the stability of anti-hCRP immobilization, anti-hCRP-functionalized sensors were sequentially incubated in 0.01% BSA solution, 100 ng/mL hCRP, and 100 ng/mL biotinylated anti-hCRP. Assuming that bare Au patches were blocked with BSA, $\Delta\lambda_{LSPR}$ detected after introducing hCRP and biotinylated anti-hCRP was explained by binding of hCRP to anti-hCRP and of biotinylated anti-hCRP to hCRP (Table 3).

The wavelength shifts measured from substrates functionalized with anti-hCRP bound through physical adsorption were 2.00, 2.25, and −3.00 nm after binding of BSA, hCRP, and biotinylated anti-hCRP, respectively. This indicates that, although both blocking buffer and hCRP bound efficiently, the final incubation in biotinylated anti-hCRP induced loss of biomolecules from the sensor surface. A primary source of biomolecule loss originates from rinsing of substrates between incubation steps and UV−vis measurements, which is observed as a blue shift since these antibodies are heavy in mass and overall neutrally charged. Thus, anti-hCRP was not strongly bound to AuNS, which was anticipated since dispersion forces are based on weak intermolecular interactions. Table 3 shows that substrates functionalized with μCP gave the most scattered results: 12.29, 2.25, and −2.88 nm. Like the adsorption method, μCP is based on weak dispersion forces, which explains negative $\Delta\lambda_{LSPR}$ after incubation in biotinylated anti-hCRP. In addition, aforementioned damage to the sensor surface by the PDMS stamp contributed to dispersion of the detected signals. Immobilization methods using both MUA (1.60, 5.20, 6.80 nm) and HS−PEG−COOH (2.00, 1.40, 2.60 nm) linkers resulted mostly in red shifts of $\Delta\lambda_{LSPR}$; however, the MUA method generated the most reproducible measurements. This observation can be explained by the uniform length of MUA linkers and strong Au−S covalent interactions that efficiently hold anti-hCRP on the AuNS surface.[48] HS−PEG−COOH linkers are commonly characterized by average weight since the length of individual molecules varies.[49] Various lengths of individual PEG linkers lead to slightly more scattered measurements when compared to uniformly long MUA linkers. One possible explanation for this is that, since PEGylated linkers are not equal in length, the extinction coefficient around each nanostructure is somewhat different,[50] whereas MUA molecules consist of 11 $-CH_2-$ units ensuring a uniform distance between anti-hCRP and AuNS. In addition, an adequate distance between the biomolecule and the substrate surface assures that this molecule retains its overall shape and conformation. Optimal distance between the nanostructure surface and the immobilized biomolecule varies depending on a number of parameters including size, shape, and dielectric constants of both the nanostructure and the biomolecule.[51,52] According to our findings, anti-hCRP bound to AuNS via MUA linkers remains bioactive, which implies that the spacing between the antibody and AuNS is sufficient. Since this method resulted in the highest $\Delta\lambda_{LSPR}$ after exposing anti-hCRP-coated AuNS to hCRP, and later to biotinylated anti-hCRP, we concluded that this immobilization strategy leads to the most efficient immobilization of anti-hCRP and ensures these antibodies remain attached to the sensor surface throughout a sandwich-type immunoassay.

In addition, we tested HS−PEG−COOH and MUA coverage uniformity by measuring the mean fluorescence intensity of sensors functionalized with fluorescent streptavidin dye. Figures S3 and S4 show confocal microscopy images of these sensor surfaces and normalized fluorescence intensity plots, respectively. We found that streptavidin dye immobilized via MUA surface chemistry had higher fluorescence intensity (i.e., higher concentration) and smaller standard deviation (i.e.,

DOI: 10.1021/acs.analchem.9b03780
Anal. Chem. 2019, 91, 15090−15098

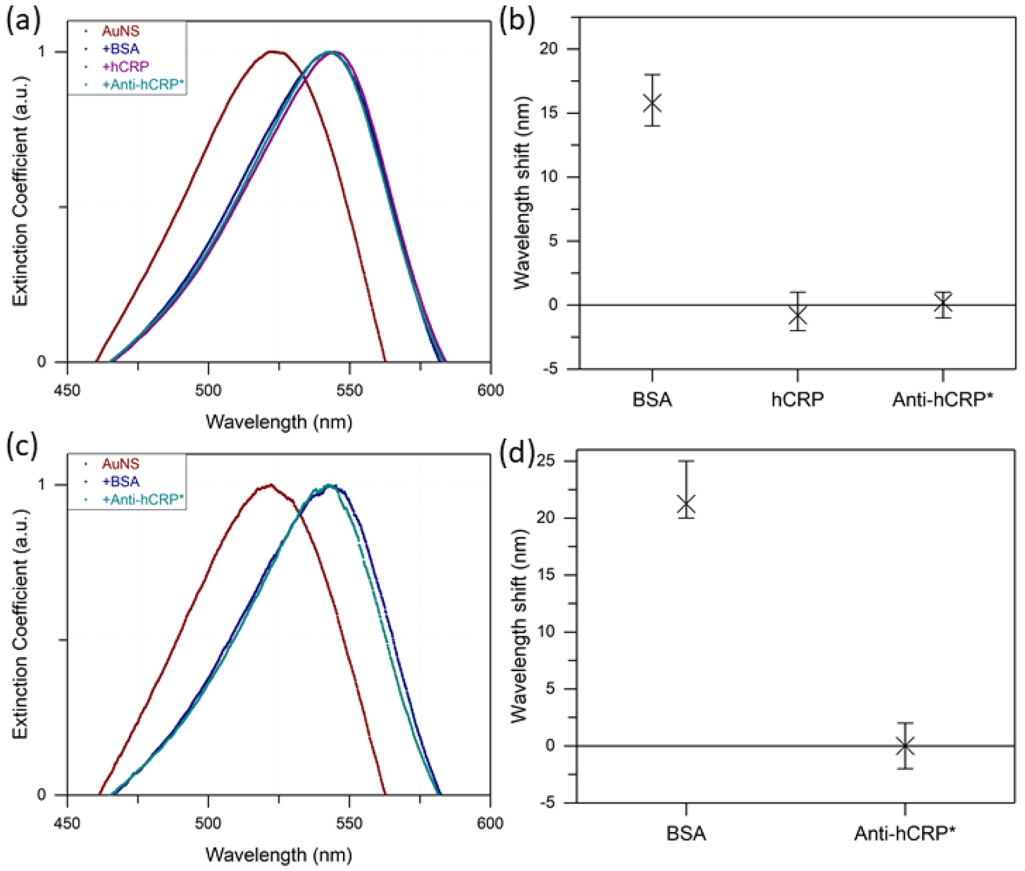

Figure 6. (a) UV−vis spectra recorded from bare Au nanostructures (red), after blocking the surface with BSA (blue), after incubation in hCRP (purple), and after incubation in biotinylated anti-hCRP (teal). (b) Control 1: $\Delta\lambda_{LSPR}$ (nm) detected after incubation of BSA-blocked bare substrate in hCRP and biotinylated anti-hCRP. (c) UV−vis spectra recorded from bare Au nanostructures (red), after blocking the surface with BSA (blue), and after incubation in biotinylated anti-hCRP (teal). (d) Control 2: $\Delta\lambda_{LSPR}$ (nm) after incubation of BSA-blocked bare substrate in biotinylated anti-hCRP.

Table 2. $\Delta\lambda_{LSPR}$ Measured in Negative Control Systems after Exposing BSA-Blocked AuNS to hCRP, Biotinylated anti-hCRP (anti-hCRP*) in Control 1, and Only Biotinylated anti-hCRP (anti-hCRP*) in Control 2

$\Delta\lambda_{LSPR}$ (nm)	BSA	hCRP	anti-hCRP*
control 1	15.8 ± 1.6	−0.80 ± 1.2	−0.20 ± 0.8
control 2	21.25 ± 2.2		0.0 ± 1.4

better uniformity). As a consequence, the MUA immobilization method has the most reliable results in the efficiency and stability analysis tests. Although the MUA immobilization method resulted in the most reproducible measurements, it has not been previously quantitatively compared to other Au surface functionalization methods. Therefore, despite of this method being quite time-consuming, it is recommended for immobilization of biomolecules on nonspherical plasmonic Au nanostructures.

Sensor Specificity, LOD, and LOQ. Although the MUA method efficiently binds anti-hCRP to AuNS and ensures the antibody stays attached to the sensor surface throughout the immunoassay, it does not necessarily guarantee that anti-hCRP remains specific solely to its antigen, hCRP. To test its specificity, after treating the surface of the anti-hCRP-coated substrate with 0.01% BSA, 100 ng/mL IL-6 was introduced onto the sensor surface instead of its specific hCRP. Incubation of anti-hCRP-coated AuNS substrates in IL-6 resulted in negligible $\Delta\lambda_{LSPR}$, suggesting that anti-hCRP immobilized using MUA method retains its specificity to hCRP (see Figure 7 and Table 4).

The final test performed to characterize the sensor surface functionalized with anti-hCRP using the MUA method was estimation of its LOD and LOQ. Sensors with anti-hCRP attached to their surfaces were incubated in five different concentrations of hCRP (Figure 8).

Table 3. $\Delta\lambda_{LSPR}$ Detected after Blocking with 0.01% BSA, Incubation in 100 ng/mL hCRP, and 100 ng/mL Biotinylated anti-hCRP (anti-hCRP*)[a]

$\Delta\lambda_{LSPR}$ (nm)	adsorption	μCP	MUA	HS−PEG−COOH
BSA	2.00 ± 2.35	12.29 ± 6.61	1.60 ± 1.36	2.00 ± 3.52
hCRP	2.25 ± 5.31	2.25 ± 2.77	5.20 ± 1.83	1.40 ± 1.02
anti-hCRP*	−3.00 ± 4.06	−2.88 ± 4.91	6.80 ± 1.17	2.60 ± 2.42

[a]Sensor functionalization using MUA linkers leads to the highest hCRP and anti-hCRP immobilization results.

DOI: 10.1021/acs.analchem.9b03780
Anal. Chem. 2019, 91, 15090−15098

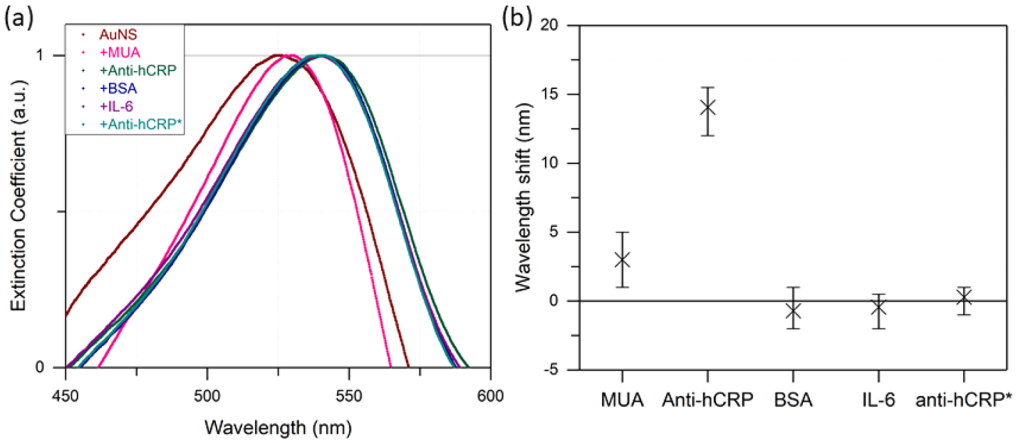

Figure 7. Specificity analysis: (a) UV−vis spectra recorded from bare Au nanostructures (red), after introducing MUA linkers (pink), after incubating in anti-hCRP (green), further blocking with BSA (blue), incubating in nonspecific IL-6 (purple), and biotinylated anti-hCRP (teal). (b) $\Delta\lambda_{LSPR}$ (nm) averaged over eight runs of incubation of substrates functionalized with anti-hCRP in 100 ng/mL IL-6; anti-hCRP immobilized on Au nanostructures using MUA linkers did not bind to nonspecific IL-6 or biotinylated anti-hCRP (anti-hCRP*).

Table 4. $\Delta\lambda_{LSPR}$ after Functionalization of AuNS with 100 ng/mL anti-hCRP Using the MUA Method, Later Incubated in 0.01% BSA, 100 ng/mL Nonspecific IL-6 (1.5 h, 4 °C), and 100 ng/mL Biotinylated anti-hCRP (anti-hCRP*; 1.5 h, 4 °C)

incubation step	MUA	anti-hCRP	BSA	IL-6	anti-hCRP*
$\Delta\lambda_{LSPR}$ (nm)	3.00 ± 1.3	14.1 ± 1.1	−0.71 ± 0.9	−0.44 ± 0.8	0.29 ± 0.7

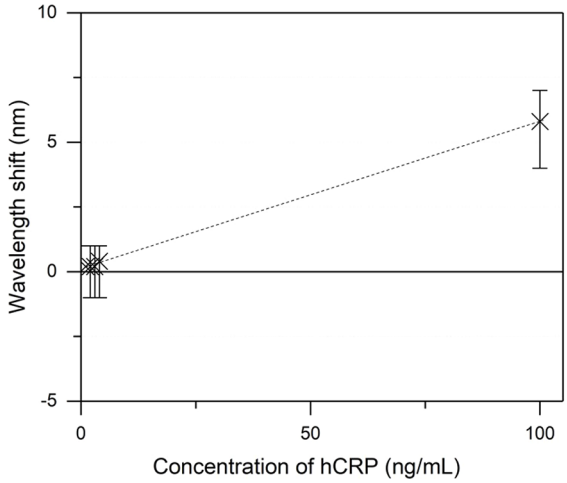

Figure 8. LOD calculations: sensors functionalized with anti-hCRP were incubated in five different concentrations of hCRP (100 pg/mL, 1 ng/mL, 10 ng/mL, 100 ng/mL, and 1 μg/mL). The mean values of $\Delta\lambda_{LSPR}$ were plotted against hCRP concentrations, and LOD was found to be equal to 41.0 ng/mL.

To calculate limits of detection and quantification of the functionalized sensor surface, we used a standard approach by plotting dependence of $\Delta\lambda_{LSPR}$ on the measured concentration of hCRP and calculated LOD and LOQ according to the standard formulas:[53]

$$\mathrm{LOD} = \left(\frac{\text{standard error}}{\text{slope}}\right)3.3 \quad (3)$$

$$\mathrm{LOQ} = \left(\frac{\text{standard error}}{\text{slope}}\right)10 \quad (4)$$

Figure 8 demonstrates a relationship between $\Delta\lambda_{LSPR}$ (nm) and concentration of hCRP in nanograms per milliliter. Since only the first four data points were in a linear regime, we plotted a standard addition line as a calibration curve by using those points and got the following equation: $y = 0.0561x + 0.1933$, where slope = 0.0561 ng/mL indicates the sensitivity of the fabricated sensors. Standard error was calculated using the STEYX function in Excel and was found to be equal to 0.6967 ng/mL. By inserting these values, we calculated LOD and LOQ according to eqs 3 and 4 and found them to be equal to 41.0 and 124.2 ng/mL, respectively. Calculated limits are comparable to those of previously reported studies when Au nanoparticles were used for biosensing of hCRP (e.g., LOD = 19 ng/mL)[54] and are significantly lower than the working protein concentrations, which is why resolution of measured signals can be justified.[55]

Lastly, to test the efficiency of the MUA immobilization method for biosensing applications, we performed an immunoassay with anti-hCRP as a primary antibody and human serum spiked with 100 ng/mL hCRP as an antigen. Mean $\Delta\lambda_{LSPR}$ after introducing the hCRP-spiked human serum sample was calculated to be 4.86 ± 0.64, whereas mean $\Delta\lambda_{LSPR}$ after incubation in pure 100 ng/mL hCRP was equal to 5.20 ± 1.83 (p-value = 0.46, α = 0.05). Both hCRP-spiked human serum and pure hCRP samples display similar wavelength shifts, implying that MUA surface chemistry is an efficient method for immobilizing biomolecules on nonspherical Au nanostructures for complex biological sample sensing applications.

CONCLUSIONS

Herein, we compared four representative surface chemistry methods exploited for immobilization of biomolecules on Au nanostructures and estimated effect of nonspherical shapes of nanostructures for LSPR biosensing applications. Protein immobilization efficiency was estimated based on the λ_{LSPR} shifts before and after incubation of AuNS in anti-hCRP. According to our findings, when nonspherical plasmonic Au nanostructures are employed for LSPR sensing, binding of

DOI: 10.1021/acs.analchem.9b03780
Anal. Chem. 2019, 91, 15090−15098

proteins via MUA linkers gives the most efficient and reproducible antibody immobilization results. Furthermore, anti-hCRP bound to the sensor surface via MUA linkers retained its specificity toward hCRP, accurately detected hCRP in human serum, and gave negligible $\Delta\lambda_{LSPR}$ after incubation in a nonspecific antigen, IL-6. Finally, LOD and LOQ of sensors functionalized using the present surface chemistry were found to be sufficiently low, 41.0 and 124.2 ng/mL. Overall, MUA surface chemistry is recommended for binding of biomolecules to nonspherical plasmonic Au nanostructures, and thus, our work reveals critical new information for efficient immobilization of biomolecules important for reliable plasmonic biosensing purposes that leads to more sensitive molecule detection and, as a consequence, to more accurate diagnostics.

■ ASSOCIATED CONTENT

Supporting Information

The Supporting Information is available free of charge on the ACS Publications website at DOI: 10.1021/acs.analchem.9b03780.

Schematic explanation of the μCP mechanism using a PDMS stamp and real images of the PDMS stamps before and after contacting with the AuNS surface, immobilization efficiency analysis supported by adding the mean fluorescence data for HS−PEG−COOH and MUA modified substrates, and ANOVA and two-sample *t* tests for estimation of statistical significance of the acquired data (PDF)

■ AUTHOR INFORMATION

Corresponding Author

*E-mail: amy.shen@oist.jp.

ORCID

Ainash Garifullina: 0000-0002-9330-0605

Amy Q. Shen: 0000-0002-1222-6264

Notes

The authors declare no competing financial interest.

■ ACKNOWLEDGMENTS

We acknowledge financial support from the Okinawa Institute of Science and Technology Graduate University (OIST) with subsidy funding from the Cabinet Office, Government of Japan. In addition, the authors thank Dr. Nikhil Bhalla who provided insight and expertise that assisted the research and Ms. Shivani Sathish for great assistance with methodology.

■ REFERENCES

(1) Freeman, S.; Sharp, J. C.; Harrington, M. *Biological Science*; Prentice Hall: Upper Saddle River, NJ, 2002; Vol. *1*.

(2) Stewart, D. E.; Sarkar, A.; Wampler, J. E. *J. Mol. Biol.* **1990**, *214*, 253−260.

(3) Alberts, B.; Bray, D.; Hopkin, K.; Johnson, A.; Lewis, J.; Raff, M.; Roberts, K.; Walter, P. *Essential Cell Biology*; Garland Science: New York, 2013.

(4) Prasad, P. N. *Introduction to Biophotonics*; John Wiley & Sons: Hoboken, NJ, 2004.

(5) Anker, J. N.; Hall, W. P.; Lyandres, O.; Shah, N. C.; Zhao, J.; Van Duyne, R. P. *Nanoscience And Technology: A Collection of Reviews from Nature Journals*; World Scientific: Singapore, 2010; pp 308−319.

(6) Rao, V. S.; Srinivas, K.; Sujini, G. N.; Kumar, G. N. *Int. J. Proteomics* **2014**, *2014*, 1−12.

(7) Arkin, M. R.; Wells, J. A. *Nat. Rev. Drug Discovery* **2004**, *3*, 301.

(8) Aschenbrenner, D.; Pippig, D. A.; Klamecka, K.; Limmer, K.; Leonhardt, H.; Gaub, H. E. *PLoS One* **2014**, *9*, e115049.

(9) Liu, Y.; Yu, J. *Microchim. Acta* **2016**, *183*, 1−19.

(10) Rao, S. V.; Anderson, K. W.; Bachas, L. G. *Microchim. Acta* **1998**, *128*, 127−143.

(11) Liu, Y.; Zhu, Z.; Wang, C.; Gao, R.; Yang, X.; Liu, S. *Analyst* **2019**, *144*, 2130−2137.

(12) Niu, L.; Zhang, N.; Liu, H.; Zhou, X.; Knoll, W. *Biomicrofluidics* **2015**, *9*, 052611.

(13) Aubé, A.; Campbell, S.; Schmitzer, A. R.; Claing, A.; Masson, J.-F. *Analyst* **2017**, *142*, 2343−2353.

(14) Ciaurriz, P.; Fernández, F.; Tellechea, E.; Moran, J. F.; Asensio, A. C. *Beilstein J. Nanotechnol.* **2017**, *8*, 244.

(15) Lee, S.; Mayer, K. M.; Hafner, J. H. *Anal. Chem.* **2009**, *81*, 4450−4455.

(16) Xu, J. X.; Siriwardana, K.; Zhou, Y.; Zou, S.; Zhang, D. *Anal. Chem.* **2018**, *90*, 785−793.

(17) Homola, J.; Yee, S. S.; Gauglitz, G. *Sens. Actuators, B* **1999**, *54*, 3−15.

(18) Lee, K.-S.; El-Sayed, M. A. *J. Phys. Chem. B* **2006**, *110*, 19220−19225.

(19) Tang, Y.; Zhang, W.; Liu, J.; Zhang, L.; Huang, W.; Huo, F.; Tian, D. *Nanoscale* **2015**, *7*, 6039−6044.

(20) Black, S.; Kushner, I.; Samols, D. *J. Biol. Chem.* **2004**, *279*, 48487−48490.

(21) Welch, N. G.; Scoble, J. A.; Muir, B. W.; Pigram, P. J. *Biointerphases* **2017**, *12*, 02D301.

(22) Sathish, S.; Ricoult, S. G.; Toda-Peters, K.; Shen, A. Q. *Analyst* **2017**, *142*, 1772−1781.

(23) Nuzzo, R. G.; Allara, D. L. *J. Am. Chem. Soc.* **1983**, *105*, 4481−4483.

(24) Häkkinen, H. *Nat. Chem.* **2012**, *4*, 443.

(25) Karyakin, A. A.; Presnova, G. V.; Rubtsova, M. Y.; Egorov, A. M. *Anal. Chem.* **2000**, *72*, 3805−3811.

(26) Bolduc, O. R.; Masson, J.-F. *Langmuir* **2008**, *24*, 12085−12091.

(27) Bhalla, N.; Sathish, S.; Galvin, C. J.; Campbell, R. A.; Sinha, A.; Shen, A. Q. *ACS Appl. Mater. Interfaces* **2018**, *10*, 219−226.

(28) Bontempi, N.; Chong, K. E.; Orton, H. W.; Staude, I.; Choi, D.-Y.; Alessandri, I.; Kivshar, Y. S.; Neshev, D. N. *Nanoscale* **2017**, *9*, 4972−4980.

(29) Love, J. C.; Estroff, L. A.; Kriebel, J. K.; Nuzzo, R. G.; Whitesides, G. M. *Chem. Rev.* **2005**, *105*, 1103−1170.

(30) Formisano, N.; Bhalla, N.; Wong, L. C. C.; Di Lorenzo, M.; Pula, G.; Estrela, P. *Electrochem. Commun.* **2015**, *57*, 70−73.

(31) Samanta, D.; Sarkar, A. *Chem. Soc. Rev.* **2011**, *40*, 2567−2592.

(32) Sun, X. *PSMA-Targeted Nano-Conjugates as Dual-Modality (MRI/PET) Imaging Probes for the Non-Invasive Detection of Prostate Cancer*; Defence Technical Information Center: Fort Belvoir, VA, 2009.

(33) Zhang, Z.; Lu, D.-F.; Liu, Q.; Qi, Z.-M.; Yang, L.; Liu, J. *Analyst* **2012**, *137*, 4822−4828.

(34) Linman, M. J.; Abbas, A.; Cheng, Q. *Analyst* **2010**, *135*, 2759−2767.

(35) Russo, V.; Michieli, N.; Cesca, T.; Scian, C.; Silvestri, D.; Morpurgo, M.; Mattei, G. *Nanoscale* **2017**, *9*, 10117−10125.

(36) Mayer, K. M.; Hafner, J. H. *Chem. Rev.* **2011**, *111*, 3828−3857.

(37) Link, S.; Mohamed, M.; El-Sayed, M. *J. Phys. Chem. B* **1999**, *103*, 3073−3077.

(38) Nehl, C. L.; Hafner, J. H. *J. Mater. Chem.* **2008**, *18*, 2415−2419.

(39) Gans, R. V. *Ann. Phys.* **1915**, *352*, 270−284.

(40) Papavassiliou, G. C. *Prog. Solid State Chem.* **1979**, *12*, 185−271.

(41) Shen, Y.; Zhou, J.; Liu, T.; Tao, Y.; Jiang, R.; Liu, M.; Xiao, G.; Zhu, J.; Zhou, Z.-K.; Wang, X.; Jin, C.; Wang, J. *Nat. Commun.* **2013**, *4*, 2381.

(42) Willets, K. A.; Van Duyne, R. P. *Annu. Rev. Phys. Chem.* **2007**, *58*, 267−297.

(43) Liu, W.; Hou, S.; Yan, J.; Zhang, H.; Ji, Y.; Wu, X. *Nanoscale* **2016**, *8*, 780−784.

(44) Xue, Y.; Li, X.; Li, H.; Zhang, W. *Nat. Commun.* **2014**, *5*, 4348.

DOI: 10.1021/acs.analchem.9b03780
Anal. Chem. 2019, 91, 15090−15098

(45) Atta, N. F.; Galal, A.; El-Ads, E. H. *Analyst* **2012**, *137*, 2658−2668.
(46) Fraire, J. C.; Motrich, R. D.; Coronado, E. A. *Nanoscale* **2016**, *8*, 17169−17180.
(47) Jeyachandran, Y.; Mielczarski, J.; Mielczarski, E.; Rai, B. *J. Colloid Interface Sci.* **2010**, *341*, 136−142.
(48) Su, S.; Zuo, X.; Pan, D.; Pei, H.; Wang, L.; Fan, C.; Huang, W. *Nanoscale* **2013**, *5*, 2589−2599.
(49) Chakrabarty, B.; Ghoshal, A.; Purkait, M. *J. Membr. Sci.* **2008**, *309*, 209−221.
(50) Marinakos, S. M.; Chen, S.; Chilkoti, A. *Anal. Chem.* **2007**, *79*, 5278−5283.
(51) Abstiens, K.; Gregoritza, M.; Goepferich, A. M. *ACS Appl. Mater. Interfaces* **2019**, *11*, 1311−1320.
(52) Verma, A.; Srivastava, S.; Rotello, V. M. *Chem. Mater.* **2005**, *17*, 6317−6322.
(53) Shabir, G. A. *Journal of chromatography A* **2003**, *987*, 57−66.
(54) Bryan, T.; Luo, X.; Bueno, P. R.; Davis, J. J. *Biosens. Bioelectron.* **2013**, *39*, 94−98.
(55) Melaine, F.; Coilhac, C.; Roupioz, Y.; Buhot, A. *Nanoscale* **2016**, *8*, 16947−16954.

DOI: 10.1021/acs.analchem.9b03780
Anal. Chem. 2019, 91, 15090−15098